

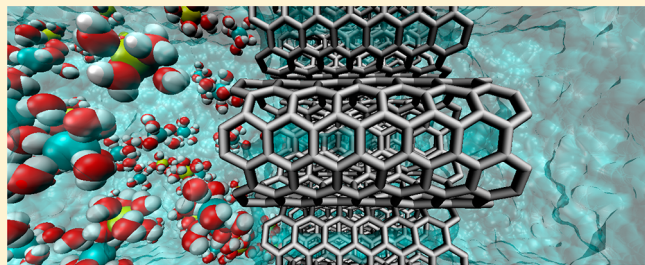
# Size Effects of Pore Density and Solute Size on Water Osmosis through Nanoporous Membrane

Kuiwen Zhao and Huiying Wu\*

School of Mechanical Engineering, Shanghai Jiao Tong University, 800 Dong Chuan Road, Shanghai, 200240, China

 Supporting Information

**ABSTRACT:** Understanding the behavior of osmotic transport across nanoporous membranes at molecular level is critical to their design and applications, and it is also beneficial to the comprehension of the mechanism of biological transmembrane transport processes. Pore density is an important parameter for nanoporous membranes. To better understand the influence of pore density on osmotic transport, we have performed systematic molecular dynamics simulations on water osmosis across nanoporous membranes with different pore densities (i.e., number of pores per unit area of membrane). The simulation results reveal that significant size effects occur when the pore density is so high that the center-to-center distance between neighboring nanopores is comparable to the solute size. The size effects are independent of the pore diameter and solute concentration. A simple quantitative correlation between pore density, solute size, and osmotic flux has been established. The results are excellently consistent with the theoretical predictions. It is also shown that solute hydration plays an important role in real osmotic processes. Solute hydration strengthens the size effects of pore density on osmotic processes due to the enlarged effective solute size induced by hydration. The influence of pore density, solute size, and solute hydration on water osmosis through nanoporous membranes can be introduced to eliminate the deviations of real osmotic processes from ideal behavior.



## INTRODUCTION

Osmosis is fundamental and important for many biological processes. For instance, osmotic water regulation by cell membranes is essential for all life forms throughout nature. Osmotically driven transport has wide applications, including power generation by pressure retarded osmosis,<sup>1</sup> osmotically controlled drug release and delivery,<sup>2</sup> osmotic microactuator and micropump for microfluidic devices,<sup>3–5</sup> and forward osmosis water treatment, desalination,<sup>6</sup> and food processing,<sup>7,8</sup> etc.

High permeability for water and excellent exclusion of solutes are important for selective transport membranes. They could lead to reduced equipment sizes and improved efficiency of membrane transport systems. Therefore, developing osmosis membranes with high solute selectivity without sacrificing water permeability is greatly demanded. However, this cannot be achieved by conventional selective permeable membranes that follow the solution-diffusion mechanism. Biology provides an inspiration for novel membranes development. Cellular transmembrane water channels aquaporins (AQPs) have high permeability and excellent selectivity characteristics for the transport of water. Developing nanoporous membranes by mimicking the transport properties of AQPs' nanopores has attracted a great deal of attention in recent years.<sup>9–11</sup> Molecular dynamics (MD) simulations have revealed that water could flow through carbon nanotube (CNT) at an ultrafast flow rate, in approximately the same magnitude to that measured through

AQP.<sup>12</sup> In agreement with the simulation results, experiments have shown that the fluxes of fluid through CNT nanoporous membranes are several orders of magnitude higher than those predicted from traditional hydrodynamic theories.<sup>13,14</sup> The ultrafast flow results from the almost frictionless surface of the carbon nanotube.<sup>15</sup> It is inferred that the main limitation appears to be the barriers at the entry and exit of the nanopores.<sup>16</sup> Consistent with this inference, MD simulations indicated that the water flux in nanotubes is independent of nanotube length within dozens of nanometers.<sup>17</sup> This can be attributed to the frictionless surface of nanotubes.

Furthermore, MD simulations have shown that the nanoporous membranes of nanotubes are capable of rejecting solute particles, while conducting water extraordinarily fast,<sup>16,18–20</sup> which was qualitatively confirmed by experimental studies.<sup>21</sup> A high flow rate comparable to those measured for biological water channels was observed for water osmotic transport through CNTs.<sup>16</sup> Simulations also indicated that the mechanism of water osmotic transport does not change with the pore size if the pores are strictly semipermeable.<sup>22</sup> In reality, besides nanotubes, most nanoporous structure materials including porous graphene<sup>23,24</sup> and molecular self-assembly nanoporous structures<sup>25–27</sup> display excellent molecular sieving and ultrafast

**Received:** August 2, 2012

**Revised:** October 30, 2012

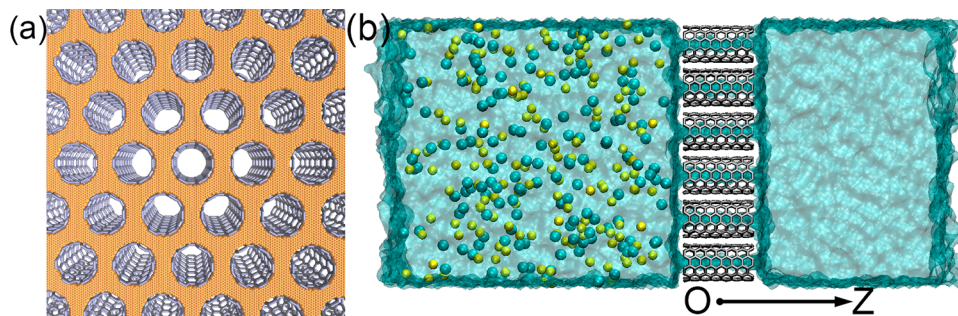


**Figure 1.** Schematic of the simulation system. (a) Snapshot of the hexagonally packed CNT (gray tubes) membrane. The large gap between the nanotubes is filled with the graphene sheets (brown) at the two ends of the nanotubes. (b) CNT membrane (gray tubes in the middle) separates NaCl solution (left, blue-green transparent liquid with ions shown by particles in it) and pure water (right, blue-green transparent liquid). The osmotic pressure drives water to flow from the right pure water reservoir to the left solution reservoir.

transport properties, offering exciting possibilities for the extensive practical applications.

Inspired by the exciting possibilities shown by nanoporous membranes, researchers are beginning to focus on their fabrications. Advanced nanofabrication techniques have opened up new possibilities for the development of nanoporous membranes with high throughput and perfect selectivity. Nanoporous membranes with a high pore density (i.e., number of pores per unit area of membrane) can be produced by several fabrication methods. Large areas of CNT membranes with a pore density of at least  $1 \times 10^{13}$  pores/cm<sup>2</sup> have been successfully synthesized by chemical vapor deposition.<sup>28–31</sup> The pore density can be further increased to  $10^{14}$  pores/cm<sup>2</sup> by reducing nanotube diameter.<sup>31</sup> The center-to-center distance between neighboring pores (for simplicity, “distance between pores” is used instead in the following sections) is almost close to 1 nm. Protein-based nanoporous membranes with a mean distance between pores of approximately 10 nm can be obtained via self-assembly.<sup>25</sup> More recently, nanoporous graphene sheets with a pore density of  $5.1 \times 10^{11}$  pores/cm<sup>2</sup> have been successfully fabricated by electron and ion beam-induced damage in graphene-based materials with atomic precision.<sup>32</sup> With the rapid development of nanofabrication techniques, the pore density of nanoporous membranes is anticipated to be increased further.

In addition to the pore density, the size of solute changes greatly depending on its type. The diameter of ordinary solutes in solution increases from several angstroms (e.g., 0.668 nm for Li<sup>+</sup> ion<sup>33</sup>) up to several nanometers (e.g., 8 nm for albumin<sup>34</sup>). Significant size effects may occur during osmotic processes if the pores are very close with each other or the solute size is relatively large. This has not been considered in previous studies though a very small distance between pores of less than 2.8 nm (pore density  $>1.5 \times 10^{13}$  pores/cm<sup>2</sup>) is set in these works to reduce the computational cost.<sup>16,35</sup> To what extents are the influences of pore density and solute size on osmotic processes? To address this issue, we perform systematic MD simulations to study the water osmotic transport through nanoporous membranes with different pore densities. The primary goal of this work is to establish the relationship between the pore density, solute size, and water osmotic transport properties. By making this study, we intend to provide a design guide of more effective nanoporous structures to increase the efficiency and controllability of osmosis-based processes. In addition, this study will offer a better understanding of the transport features of biological transmembrane

channels, such as quaternary organized AQPS monomer, whose distance between pores is less than 3 nm.<sup>36</sup>

## METHODS

In this study, the hexagonally packed structure of pore distribution is chosen, and the uncapped (6, 6) armchair single-wall CNTs are chosen as a model of nanopores (Figure 1a). Hexagonally packed structure is chosen because it is a most frequently encountered pore distribution form for nanoporous structures. The schematic illustration of the simulation system is shown in Figure 1b. Continuous membrane is formed by employing periodic boundaries. The NaCl solution and pure water reservoirs are separated by this membrane. Vacuum chambers exist at the left and right sides of the simulation box, avoiding the mixing of pure water and solution. The length and diameter of the nanotubes are 16.0 and 8.1 Å, respectively. The narrow inner channels of the nanotubes permit the passage of water molecules, but reject Na<sup>+</sup> and Cl<sup>-</sup> ions. The osmotic pressure drives water to flow from the pure water reservoir to the solution reservoir. The concentration of NaCl in the solution reservoir is 1.1 mol/L. A low concentration of NaCl solution is selected owing to two reasons. First, it is frequently encountered in biological processes and industrial applications. Second, the hydration structure of ions can be affected by the neighboring ions at high concentration. The condition of low concentration will be of great benefit to the quantitative study.

MD simulations were performed using NAMD<sup>37</sup> and visualized using VMD.<sup>38</sup> A time step of 2 fs was used. Temperature was maintained at 300 K by using Langevin thermostat. Pressure was maintained at 1 atm by using Nosé–Hoover Langevin piston method. Periodic boundary conditions were applied in all directions. Particle Mesh Ewald summation was used for the calculation of the long-range electrostatic Coulomb interaction. CHARMM27 force field parameters<sup>39</sup> and the TIP3P water model<sup>40</sup> were used for all simulations. Force constants of carbon atoms were defined as those of aromatic carbons (CA) in the CHARMM27 force field. All the bonds and angles in the simulation systems were held rigid with the SHAKE algorithm. The van der Waals parameters of different species of atoms were obtained by the Lorentz–Berthelot combining rules. A 12-Å cutoff distance for pair interactions was used. The simulation box ranges from  $6.24 \times 6.0 \times 20.0$  to  $8.31 \times 7.2 \times 20.0$  nm<sup>3</sup>, depending on the number of CNTs and center-to-center distance between neighboring CNTs. Harmonic restraining force of 1.0 kcal/mol/Å<sup>2</sup> was applied to all of the carbon atoms in the simulations to prevent the nanotubes out-of-plane displacement. In all the simulations

here, the membranes remained stable, with less than 2% fluctuations during the total run time. In all cases, structures were saved every 1 ps. Equilibrium density of bulk pure water is around 1.009 g/cm<sup>3</sup>. A density of 1.009 g/cm<sup>3</sup> at 1 atm for TIP3P water in CHARMM27 force field corresponds well to the result in ref 41, which used the same simulation methods.

## RESULTS AND DISCUSSION

In order to investigate the influence of the pore density of nanoporous membranes on water osmotic processes, we conducted four simulations with nanotubes membranes ranging in the distance between pores from 1.2 to 2.4 nm, corresponding to the pore density from  $8.0 \times 10^{13}$  pores/cm<sup>2</sup> to  $2.0 \times 10^{13}$  pores/cm<sup>2</sup>. The numbers of uncapped nanotubes in four simulation cases are 30, 24, 16, and 12. In all cases, an equilibration time of 10 ns is needed to obtain a uniform NaCl concentration profile in the bulk solution region. The simulation data are collected after the equilibration time. The simulations are performed with a total data collection time of 1600–2400 ns·tube, which is much longer than that in previous works<sup>10,35</sup> and ensures the precision of this work. Here we define the permeation event as a water molecule entering one end of the nanotube and leaving from the opposite end. During the data collection time of each case, more than 10000 water molecules permeated through the nanotubes, yielding a net osmotic flow of about 1500 water molecules. Figure 2 shows

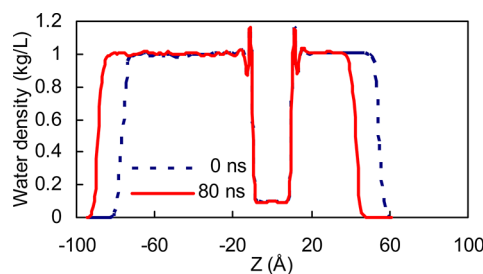


**Figure 2.** Water density profiles along the direction perpendicular to the CNT membrane at the start and the end of the data collection time. The center of the CNT membrane in Z-direction is 0 Å. The density is measured by averaging the water molecules within a 2-Å thick slab over 0.5 ns.

the water density profiles perpendicular to the membrane surface at the start and end of the data collection time of a simulation case. The bulk regions of pure water and salt solution are more than 30 Å in Z-direction during the total data collection time. This is sufficient to avoid the edge effects that can occur if the surface and interface regions of one liquid reservoir contact with each other.

The water diffusive flow is defined as the total bidirectional permeation event of water molecules between the pure water and the solution reservoirs. The water osmotic flow is defined as the net flow of water molecules from the pure water reservoir to the solution reservoir. The flux is defined as the flow of water molecules per pore per ns. Interestingly, the water osmotic flux decreases greatly with the decreasing distance between pores (Figure 3a) while the diffusive flux is nearly independent of the distance between pores (Figure 3b). No more than 1.5% difference is observed for the water diffusive flux for four simulation cases.

In order to examine whether there is any osmotic flux difference caused by the concentration difference, the NaCl

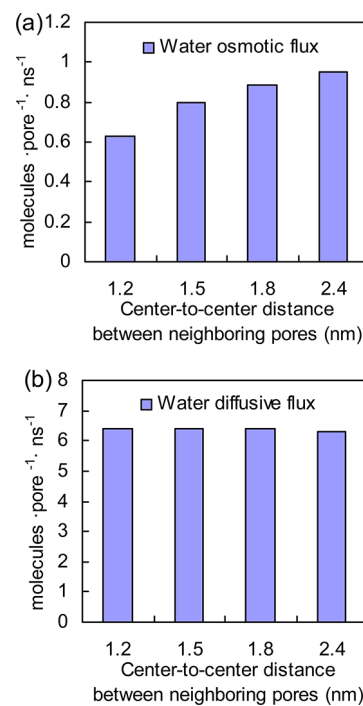


**Figure 3.** Histogram comparison of water osmotic flux and diffusive flux (molecules·pore<sup>-1</sup>·ns<sup>-1</sup>) through CNT membranes with different center-to-center distance between neighboring pores. (a) The osmotic flux decreases markedly with the decreasing center-to-center distance between neighboring pores. (b) The diffusive flux is nearly independent of the center-to-center distance between neighboring pores.

concentration is averaged over the total data collection time for each case. Figure 4 shows the average NaCl concentration

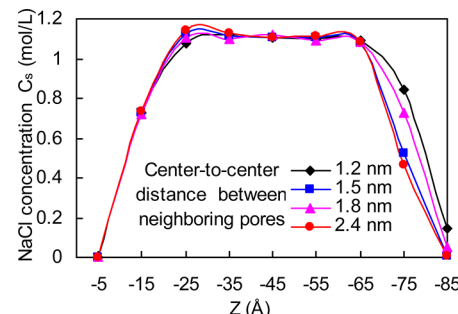


**Figure 4.** Average NaCl concentration profiles along the direction perpendicular to the CNT membranes with different center-to-center distance between neighboring pores. The center of membranes in Z-direction is 0 Å. The concentration is measured by averaging the NaCl within a 10-Å thick slab over the total data collection time for each case.

profiles along the direction perpendicular to the CNT membranes. As shown in Figure 4, there are nearly the same concentration profiles in the bulk solution region and near the surface of the membranes for total four cases. The salt concentration difference between four cases is 1% in the bulk solution region and no more than 3% near the membrane surface. Consequently, it can be concluded that very little difference in osmotic flux is caused by the difference in NaCl concentration. It should be noted that the length of the bulk solution layer with a uniform NaCl concentration profile in Z-

direction is more than 40 Å and this ensures a stable chemical potential difference between the pure water and the solution reservoirs.

**Mechanism of the Influence of Pore Density on Water Diffusion and Osmosis.** As previously introduced, the water diffusive flow means the bidirectional permeation event of water molecules through CNTs. It results from the thermal stochastic motion of water molecules. The water osmotic flow is the net flow of water molecules from the pure water reservoir to the solution reservoir, which comes from the difference in the unidirectional diffusive flows in two opposite directions through CNTs. It is caused by the asymmetry of the force on the water molecules in CNTs in two opposite directions along the channel axis, which is due to the stochastic collisions of solute particles with nanopores in membrane in the solution reservoir. That is to say, the osmotic flux is directly proportional to the frequency of the collision between solute particles and nanopores. For the nanoporous membranes with a low pore density, the pores are very far from each other. The interaction between solute particles and each pore can be regarded as an independent random event. Consequently, the osmotic flux through one pore is twice that through two pores. However, provided that the pores are very close with each other or the solute sizes are very large, collisions of ions with one pore and the pore's neighboring pores cannot be regarded as independent random events but show strong interference. A schematic illustration of the interference process is shown in Figure 5. Parts a and b of Figure 5 show two independent random events for the collision of solute particles with one pore. Both the two random events can happen at the same time if the pores in membrane are far away with each other. However, as shown in Figure 5c, the two random events above

cannot happen at the same time on the condition that the two pores are too close with each other. Obvious interference exists between the two solute particles close to the pores, which is highlighted in Figure 5d. These collision interferences lead to a decrease in the frequency of collisions between the solutes and nanopores, and consequently, the osmotic flux through each nanopore is decreased by this interference effect.

On the other hand, diffusion is a transport phenomenon resulting from the thermal stochastic motion of water molecules. The size of water molecules is greatly smaller than solute size (about a tenth in projective area in this work). Thus, there is no observable interference between the collisions of water molecules with nanopores. Therefore, water diffusive flux remains unchanged with decreasing distance between pores.

To confirm the conclusions here further, we performed MD simulations to study osmotic transport by simulating osmotic pressure with hydrostatic pressure difference,<sup>42</sup> which is a widely used method to study osmosis. The results show that nearly no difference (within 1%) exists in water osmotic flux under the same hydrostatic pressure difference for the CNT membranes used in this paper. Thus, we can conclude that the size effects of osmotic flux are due to the non-negligible solute size.

**Ionic Radius Determination.** The ionic size will exert an influence on the osmotic flow as the pore density of nanoporous membrane increases to a certain degree. Thus, the determination of ionic radius is important. The ionic crystal radius is customarily to be used as ionic radius. In reality, the ions in solution are hydrated by water molecules. The large electric field around the ions leads to the reorientation of the dipolar water molecules in their first hydration shells (Figure 6). The interaction between an ion and the surrounding water

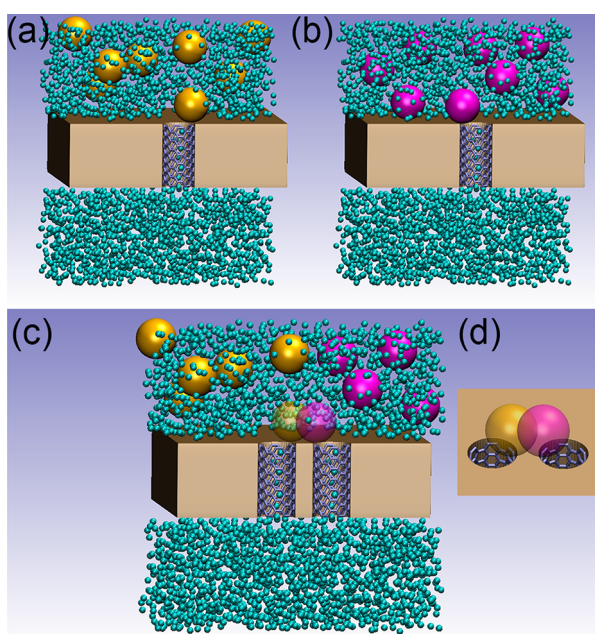


**Figure 5.** Schematic illustration (not to scale) of collision interference. Brown membranes with pores in them are nanoporous membranes. The large and small particles are solute and solvent, respectively. Parts a and b show two independent random events for the collision of ions with one pore. Part c shows the collision interference between the two ions close to the pores, which is highlighted in part d, when the two pores in parts a and b are too close with each other.

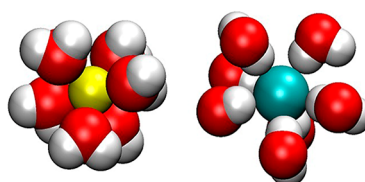


**Figure 6.** Microscopic configurations of hydrated  $\text{Na}^+$  (yellow) and  $\text{Cl}^-$  (cyan) ions. Water molecules (in the hydration shells around the ions) rearrange themselves induced by the electric field created by the ions. The hydrated ions behave as rigid spheres.

molecules in its first hydration shell is sufficiently strong. Water molecules are bound to the ion so tightly that they cannot act as free solvent water. The ion's first hydration shell behaves like a rigid sphere.<sup>43</sup> Therefore, the radius of an ion and its first hydration shell of water molecules is the effective ionic radius in aqueous solution. The physical properties of salt solutions, the behavior of ionic mobility, and the ionic selectivity of membrane channels are closely correlated with ionic hydration and effective ionic radius.<sup>33</sup> The effective ionic radius and hydration can be introduced to eliminate the deviation of aqueous solutions from ideal behavior: properties such as freezing point, boiling point, and viscosity.<sup>44,45</sup> In agreement with the phenomenal studies, experimental researches have also revealed that the ions with their first hydration shells should be regarded as rigid spheres, so that some hydrodynamic properties of solution can be modeled by describing the solution as bulk liquid water with the suspended spheres of hydrated ions.<sup>46</sup>

The radii of hydrated  $\text{Na}^+$  and  $\text{Cl}^-$  in aqueous solutions have been determined by neutron diffraction experiments to be 3.72 and 4.54 Å, respectively, which correspond to 5.1 and 6.8 hydration numbers,<sup>47</sup> the number of water molecules strongly bound to the solute in its first hydration shell. These results also have been confirmed by MD simulations.<sup>33</sup>

**Relation between Osmotic Flux, and Ionic Radius and Pore Density.** In order to quantitatively study the relationship between the osmotic flux and the pore density and ionic radius, we define the membrane area per pore,  $A_{mpp}$ , as the membrane surface area divided by the total number of pores in this membrane, i.e., the reciprocal of pore density. Then the area ratio  $A_{ion}/A_{mpp}$  is defined as the ratio of the projective area per ion,  $A_{ion}$ , to the membrane area per pore,  $A_{mpp}$ . According to previous discussion, provided that the pores are very close with each other or the solute sizes are very large, the osmotic flux decreases owing to the interference of collisions of ions with one pore and the pore's neighbor pores. It is reasonable to infer that both the decrease of membrane area per pore and the increase of projective area per ion have the same influence on osmotic flux. Thus, the area ratio  $A_{ion}/A_{mpp}$  is selected as a parameter to study the total influence of the pore density and ionic radius on water osmotic flux.

It is found from our simulations that a perfect linear relationship exists between the water osmotic flux of (6, 6) CNT and the area ratio  $A_{ion}/A_{mpp}$  (Figure 7a). To confirm this

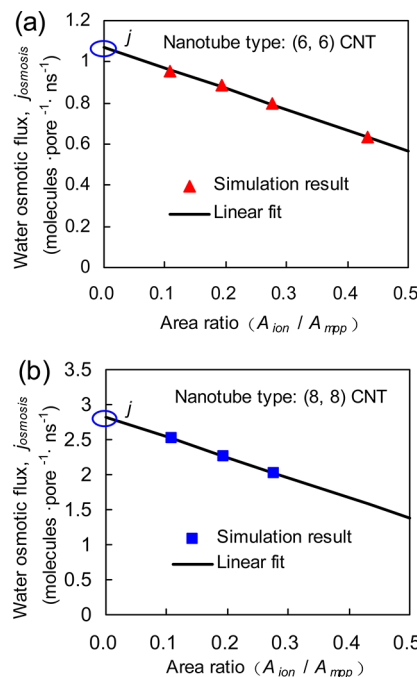


**Figure 7.** Comparison of water osmotic flux ( $\text{molecules}\cdot\text{pore}^{-1}\cdot\text{ns}^{-1}$ ) as a function of the area ratio (the ratio of projective area per ion to membrane area per pore). (a) Nanotube type is (6, 6) CNT. (b) Nanotube type is (8, 8) CNT.

phenomenon, we performed three additional simulations with (8, 8) CNT membranes (pore diameter = 10.9 Å; pore distance = 1.5, 1.8, and 2.4 nm; NaCl concentration = 1.0 mol/L; net osmotic flow ≈ 3000 water molecules; other setups are the same with the corresponding simulation cases of (6, 6) CNT membranes). The results show similar linear relationship (Figure 7b).

The ideal osmotic fluxes,  $j$ , through a single pore of (6, 6) CNT and (8, 8) CNT are predicted to be 1.07 and 2.82 water molecules per pore per ns, respectively, by extrapolating the linear fitting lines of simulation results to the points corresponding to the area ratio of 0 (shown with ellipses in Figure 7). Now we define the osmotic flux ratio  $j_{osmosis}/j$  as the ratio of the real osmotic flux through a single pore with the area ratio of  $A_{ion}/A_{mpp}$  to the ideal osmotic flux through a single pore with the  $A_{ion}/A_{mpp}$  of 0. According to the optimal linear fitting method, two linear fitting lines in Figure 7 can be expressed as  $j_{osmosis}/j = 1 - 0.94(A_{ion}/A_{mpp})$  (correlation coefficient = 0.998) and  $j_{osmosis}/j = 1 - 1.02(A_{ion}/A_{mpp})$  (correlation coefficient = 0.999), respectively. Considering the influence by the simulation errors (3.6%) that come from statistical fluctuation in osmotic flow and the determination errors of ionic radius, two linear fitting lines in Figure 7 can be correlated as a common equation as follows:

$$j_{osmosis}/j = 1 - A_{ion}/A_{mpp} \quad (1)$$

Figure 8 gives the comparison of eq 1 with the simulation results. As seen from Figure 8, eq 1 is in a good agreement with

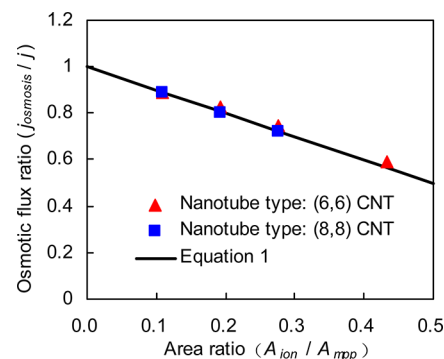


**Figure 8.** Comparison of water osmotic flux ratio ( $j_{osmosis}/j$ ) as a function of the area ratio (the ratio of the projective area per ion to the membrane area per pore).

the simulation results with a mean relative deviation of 1.1% and a linear correlation coefficient of 0.994. Accordingly, we can arrive at a conclusion that the reduction percent of osmotic flux through a single nanopore owing to the size effects of pore density and solute size is directly proportional to the area ratio  $A_{ion}/A_{mpp}$ . By the way, the predicted ideal osmotic flux through a single pore of (6, 6) CNT and (8, 8) CNT of 1.07 and 2.82 water molecules per pore per ns, respectively, can be theoretically verified, which will be discussed in the next section.

**Theoretical Description of Osmotic Transport through a Nanopore.** The continuous-time random walk (CTRW) model has been proposed to quantitatively describe the transport properties of the single-file water in nanopores.<sup>48</sup> Since osmosis is a thermodynamically driven diffusion-based process, the relationship between the water diffusion and osmosis through single-file water channels can be described by the CTRW model and thermodynamic laws.<sup>16,42</sup> The osmotic flux is determined by the bidirectional hopping rate  $k$  and the chemical potential difference of water between the solutions at two sides of the nanoporous membrane, which can be expressed by<sup>16</sup>

$$j = k \tanh\left(-\frac{\Delta\mu_w}{2k_B T}\right) \quad (2)$$

where  $j$  is the ideal osmotic flux through a single pore ( $\text{molecules}\cdot\text{pore}^{-1}\cdot\text{ns}^{-1}$ );  $k$  is the bidirectional hopping rate ( $\text{ns}^{-1}$ );  $\Delta\mu_w$  is the chemical potential difference of water molecules between the solutions at two sides of the nanoporous membrane;  $k_B$  is Boltzmann's constant;  $T$  is the absolute temperature.

The chemical potential difference of water molecules between solution 1 (high solute concentration) and solution 2 (low solute concentration) is given by

$$\Delta\mu_w = \mu_{w,1} - \mu_{w,2} = k_B T \ln\left(\frac{x_{w,1}}{x_{w,2}}\right) \quad (3)$$

where  $x_{w,1}$  and  $x_{w,2}$  are the mole fractions of free solvent water in solutions 1 and 2, respectively. As discussed previously, the interaction between an ion and the water molecules in its first hydration shell is strong, water molecules are bound to the solute so tightly that they are not acting as free solvent. Solute hydration does not change the number of solute particles, but decrease the number of water molecules acting as free solvent water. Therefore, the mole fraction of free solvent water  $x_w$  is represented by<sup>45</sup>

$$x_w = \frac{C_w - iC_s H_n}{C_w - iC_s H_n + iC_s} \quad (4)$$

where  $C_w$  and  $C_s$  are the molar concentration of water and original solute substance, respectively;  $H_n$  is the hydration number, i.e., the number of water molecules strongly bound to a solute particle; and  $i$  is the van't Hoff factor, i.e., the number of solute particles produced by the dissociation of one original solute molecule, 2 for NaCl and 1 for nonelectrolytes. The mean hydration number of ions in dilute NaCl aqueous solution is 5.95, which has been discussed in the previous paragraphs. The term  $iC_s H_n$  is the hydrated water molecules tightly bound to ions, i.e., the decreased free solvate water owing to solute hydration.

Substituting eq 3 into eq 2, the net osmotic flux is given by

$$j = k \frac{x_{w,2} - x_{w,1}}{x_{w,2} + x_{w,1}} \quad (5)$$

In this study,  $x_{w,1}$  and  $x_{w,2}$  are 95.0% and 100%, respectively. The (6, 6) CNT with a length of 16 Å is occupied by average  $N = 6.15$  water molecules in single file. The observed bidirectional permeation event  $Q$  is 6.37 per pore per ns. The bidirectional hopping rate  $k$  can be obtained to be 45.5 per ns by  $k = (N + 1) Q$ .<sup>49</sup> Then, according to eq 5, the osmotic flux is calculated to be 1.17 water molecules per pore per ns. This result corresponds well to 1.07 per pore per ns, which is obtained by the linear extrapolating of the simulation results in the preceding section.

According to the collective diffusion model,<sup>50</sup> which is not limited to the description of the single-file water transport process, eq 2 can be replaced with  $j = -D_n \Delta\mu_w / k_B T$ , where  $D_n$  is the collective diffusion coefficient of water inside the nanopore. Collective diffusion coefficient  $D_n$  obeys the Einstein relation:  $\langle n^2(t) \rangle = 2D_n t$ ,<sup>50</sup> where  $\langle n^2(t) \rangle$  is the mean square displacement (MSD) of the collective diffusion coordinate  $n(t)$  along nanopore.  $n(t)$  can be computed by integrating the instantaneous diffusion displacement  $dn(t)$ , which is defined as

$$dn(t) = \sum_{i \in S(t)} (Z_i(t) - Z_i(t - \delta t))/L \quad (6)$$

where  $L$  is the length of nanopore;  $Z_i(t)$  and  $Z_i(t - \delta t)$  are the  $Z$  coordinates of water molecule  $i$  at time  $t$  and  $t - \delta t$ , respectively, and the sum is over all the water molecules in the nanopore at time  $t$ . Equilibrium MD simulations of more than 1000 ns·tube were performed to calculate the collective diffusion coefficient  $D_n$ . The MSDs of  $n(t)$  for water in (6, 6) CNT and (8, 8) CNT are presented in Figure 9.  $D_n$  for water in

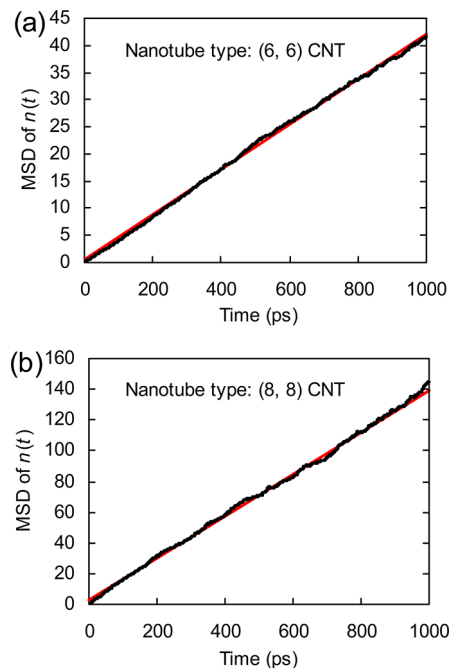


**Figure 9.** Mean square displacements (MSDs) of the water collective diffusion coordinate  $n(t)$  obtained from equilibrium MD simulations. A best linear fitting line is superimposed on each MSD curve. MSDs of  $n(t)$  show perfect linear relationships with time. (a) Nanotube type is (6, 6) CNT. (b) Nanotube type is (8, 8) CNT.

(6, 6) CNT and (8, 8) CNT are determined to be 20.8 and 68.0 per ns, respectively. Then the osmosis fluxes can be predicted to be 1.06 and 3.03 water molecules per pore per ns. These results are also corresponds well to the simulation results of 1.07 and 2.82 water molecules per pore per ns.

To verify whether the solute concentration has influence on the size effects of pore density and solute size, we performed a simulation with NaCl concentration of 0.55 mol/L and pore distance of 1.2 nm. A bidirectional permeation event of 6.40 per pore per ns and an osmotic flux of 0.31 water molecules per pore per ns are obtained. This is consistent with the prediction of eqs 1 and 5. Consequently, it can be concluded that the influence of pore distance and solute size on osmosis is independent of the solute concentration. The influence of pore density on water osmotic flux is a pore entrance effects which is supposed to be independent of the length of membrane channels. To confirm the conclusion further, we performed an additional simulation with CNT length of 3.2 nm, NaCl concentration of 1.0 mol/L, and center-to-center distance of 1.2 nm between neighboring pores. A bidirectional hopping rate of 33.1 per ns and an osmotic flux of 0.411 water molecules per pore per ns are obtained, corresponds well to the osmotic flux of 0.420 per pore per ns which is obtained by eqs 1 and 2.

With the quantitative correlation proposed in this paper, the osmotic flux of different solutions through the nanoporous membranes with different pore densities can be determined simply and precisely without extensive simulations or experiments. Assuming a pore density of  $1.5 \times 10^{13} \text{ cm}^{-2}$ , which has been successfully fabricated by chemical vapor deposition,<sup>31</sup> the nanoporous membrane of (8,8) CNTs would yield a flow rate of 0.013 m/s for 1 mol/L NaCl solution, 3 orders of magnitude higher than those obtained in current osmosis membranes.<sup>1,51</sup> It offers an exciting possibility to be served as an alternative to current commercial membranes.

## CONCLUSIONS

Many factors including solute hydration, solute size, and pore density of nanoporous membranes have influence on osmosis processes, making it deviate from the ideal behavior. Significant size effects occur when the solute size is comparable to the center-to-center distance between neighboring nanopores. The influence of pore density and solute size on osmosis is independent of pore size and solute concentration. The ionic hydration and size effects of pore density and solute size can be introduced to eliminate the deviations of real osmotic processes from ideal behavior. A simple dimensionless correlation for the real osmosis flux through a single nanopore in function of the pore density and solute size is obtained in this paper. The osmotic flux of water through the nanoporous membranes with different pore densities can be determined by this correlation. In addition, the area ratio  $A_{\text{ion}}/A_{\text{mfp}}$  is selected as a parameter in this correlation based on inference. This inference could be verified by future similar study over a variety of solute sizes.

In reality, the distributions of pores in many nanoporous membranes are nonuniform. According to the results of this work, the distribution probability of membrane surface area per pore is a necessary parameter to determine the transport properties of nanoporous membranes. The size effects of pore density and solute size on osmosis also open a new door to utilizing the nanoporous membranes in the precise determination of effective solute size, which is useful in the catalysis reaction dynamics and chemical analysis.

## ASSOCIATED CONTENT

### Supporting Information

Complete author list for ref 39. This material is available free of charge via the Internet at <http://pubs.acs.org>.

## AUTHOR INFORMATION

### Corresponding Author

\*E-mail: whysrj@sjtu.edu.cn.

### Notes

The authors declare no competing financial interest.

## ACKNOWLEDGMENTS

This work was supported by the National Natural Science Foundation of China through Grant No. 50925624, the National Basic Research Program of China (973 Program) through Grant No. 2012CB720404, and the Science and Technology Commission of Shanghai Municipality through Grant Nos. 11XD1403100 and 12JC1405100.

## REFERENCES

- (1) Achilli, A.; Cath, T. Y.; Childress, A. E. *J. Membr. Sci.* **2009**, *343*, 42–52.
- (2) Gupta, B. P.; Thakur, N.; Jain, N. P.; Banweer, J.; Jain, S. J. *Pharm. Pharm. Sci.* **2010**, *13*, 571–588.
- (3) Jensen, K. H.; Lee, J.; Bohr, T.; Bruus, H. *Lab Chip* **2009**, *9*, 2093–2099.
- (4) Su, Y. C.; Lin, L. W.; Pisano, A. P. *J. Microelectromech. Syst.* **2002**, *11*, 736–742.
- (5) Xu, Z.-R.; Yang, C.-G.; Liu, C.-H.; Zhou, Z.; Fang, J.; Wang, J.-H. *Talanta* **2010**, *80*, 1088–1093.
- (6) Elimelech, M.; Phillip, W. A. *Science* **2011**, *333*, 712–717.
- (7) Cath, T. Y.; Childress, A. E.; Elimelech, M. *J. Membr. Sci.* **2006**, *281*, 70–87.
- (8) Zhao, S.; Zou, L.; Tang, C. Y.; Mulcahy, D. *J. Membr. Sci.* **2012**, *396*, 1–21.
- (9) Hinds, B. J. *Curr. Opin. Solid State Mat. Sci.* **2012**, *16*, 1–9.
- (10) Hilder, T. A.; Gordon, D.; Chung, S.-H. *Nanomed.-Nanotechnol. Biol. Med.* **2011**, *7*, 702–709.
- (11) García-Fandiño, R.; Sansom, M. S. P. *Proc. Natl. Acad. Sci. U.S.A.* **2012**, *109*, 6939–6944.
- (12) Hummer, G.; Rasaiah, J. C.; Noworyta, J. P. *Nature* **2001**, *414*, 188–190.
- (13) Holt, J. K.; Park, H. G.; Wang, Y. M.; Stadermann, M.; Artyukhin, A. B.; Grigoropoulos, C. P.; Noy, A.; Bakajin, O. *Science* **2006**, *312*, 1034–1037.
- (14) Hinds, B. J.; Chopra, N.; Rantell, T.; Andrews, R.; Gavalas, V.; Bachas, L. G. *Science* **2004**, *303*, 62–65.
- (15) Majumder, M.; Chopra, N.; Andrews, R.; Hinds, B. J. *Nature* **2005**, *438*, 44–44.
- (16) Kalra, A.; Garde, S.; Hummer, G. *Proc. Natl. Acad. Sci. U.S.A.* **2003**, *100*, 10175–10180.
- (17) Nicholls, W. D.; Borg, M. K.; Lockerby, D. A.; Reese, J. M. *Microfluid. Nanofluid.* **2012**, *12*, 257–264.
- (18) Suk, M. E.; Raghunathan, A. V.; Aluru, N. R. *Appl. Phys. Lett.* **2008**, *92*, 133120.
- (19) Hilder, T. A.; Gordon, D.; Chung, S.-H. *Small* **2009**, *5*, 2183–2190.
- (20) Corry, B. J. *Phys. Chem. B* **2008**, *112*, 1427–1434.
- (21) Fornasier, F.; Park, H. G.; Holt, J. K.; Stadermann, M.; Grigoropoulos, C. P.; Noy, A.; Bakajin, O. *Proc. Natl. Acad. Sci. U.S.A.* **2008**, *105*, 17250–17255.
- (22) Raghunathan, A. V.; Aluru, N. R. *Phys. Rev. Lett.* **2006**, *97*, 024501.
- (23) Suk, M. E.; Aluru, N. R. *J. Phys. Chem. Lett.* **2010**, *1*, 1590–1594.
- (24) Cohen-Tanugi, D.; Grossman, J. C. *Nano Lett.* **2012**, *12*, 3602–3608.
- (25) Peng, X.; Jin, J.; Nakamura, Y.; Ohno, T.; Ichinose, I. *Nat. Nanotechnol.* **2009**, *4*, 353–357.
- (26) Kumar, M.; Grzelakowski, M.; Zilles, J.; Clark, M.; Meier, W. *Proc. Natl. Acad. Sci. U.S.A.* **2007**, *104*, 20719–20724.
- (27) Phillip, W. A.; O'Neill, B.; Rodwgin, M.; Hillmyer, M. A.; Cussler, E. L. *ACS Appl. Mater. Interfaces* **2010**, *2*, 847–853.
- (28) Yu, M.; Funke, H. H.; Falconer, J. L.; Noble, R. D. *Nano Lett.* **2009**, *9*, 225–229.
- (29) Futaba, D. N.; Hata, K.; Yamada, T.; Hiraoka, T.; Hayamizu, Y.; Kakudate, Y.; Tanaike, O.; Hatori, H.; Yumura, M.; Iijima, S. *Nat. Mater.* **2006**, *5*, 987–994.
- (30) Esconjauregui, S.; Fouquet, M.; Bayer, B. C.; Ducati, C.; Smajda, R.; Hofmann, S.; Robertson, J. *ACS Nano* **2010**, *4*, 7431–7436.
- (31) Zhong, G.; Warner, J. H.; Fouquet, M.; Robertson, A. W.; Chen, B.; Robertson, J. *ACS Nano* **2012**, *6*, 2893–2903.
- (32) Russo, C. J.; Golovchenko, J. A. *Proc. Natl. Acad. Sci. U.S.A.* **2012**, *109*, 5953–5957.
- (33) Marcus, Y. *Chem. Rev.* **2009**, *109*, 1346–1370.
- (34) Sugio, S.; Kashima, A.; Mochizuki, S.; Noda, M.; Kobayashi, K. *Protein Eng.* **1999**, *12*, 439–446.
- (35) Jia, Y.-x.; Li, H.-l.; Wang, M.; Wu, L.-y.; Hu, Y.-d. *Sep. Purif. Technol.* **2010**, *75*, 55–60.
- (36) Horsefield, R.; Norden, K.; Fellert, M.; Backmark, A.; Tornroth-Horsefield, S.; van Scheltinga, A. C. T.; Kvassman, J.; Kjellbom, P.;

- Johanson, U.; Neutze, R. *Proc. Natl. Acad. Sci. U.S.A.* **2008**, *105*, 13327–13332.
- (37) Phillips, J. C.; Braun, R.; Wang, W.; Gumbart, J.; Tajkhorshid, E.; Villa, E.; Chipot, C.; Skeel, R. D.; Kale, L.; Schulten, K. *J. Comput. Chem.* **2005**, *26*, 1781–1802.
- (38) Humphrey, W.; Dalke, A.; Schulten, K. *J. Mol. Graphics* **1996**, *14*, 33–38.
- (39) MacKerell, A. D.; Bashford, D.; Bellott, M.; Dunbrack, R. L.; Evanseck, J. D.; Field, M. J.; Fischer, S.; Gao, J.; Guo, H.; Ha, S.; et al. *J. Phys. Chem. B* **1998**, *102*, 3586–3616.
- (40) Jorgensen, W. L.; Chandrasekhar, J.; Madura, J. D.; Impey, R. W.; Klein, M. L. *J. Chem. Phys.* **1983**, *79*, 926–935.
- (41) Price, D. J.; Brooks, C. L. *J. Chem. Phys.* **2004**, *121*, 10096–10103.
- (42) Zhu, F.; Tajkhorshid, E.; Schulten, K. *Biophys. J.* **2004**, *86*, 50–57.
- (43) Laage, D.; Hynes, J. T. *Proc. Natl. Acad. Sci. U.S.A.* **2007**, *104*, 11167–11172.
- (44) Zavitsas, A. A. *J. Solution Chem.* **2010**, *39*, 301–317.
- (45) Zavitsas, A. A. *J. Phys. Chem. B* **2001**, *105*, 7805–7817.
- (46) Omta, A. W.; Kropman, M. F.; Woutersen, S.; Bakker, H. J. *Science* **2003**, *301*, 347–349.
- (47) Mancinelli, R.; Botti, A.; Bruni, F.; Ricci, M. A.; Soper, A. K. *J. Phys. Chem. B* **2007**, *111*, 13570–13577.
- (48) Berezhkovskii, A.; Hummer, G. *Phys. Rev. Lett.* **2002**, *89*, 64503.
- (49) Zhu, F.; Schulten, K. *Biophys. J.* **2003**, *85*, 236–244.
- (50) Zhu, F.; Tajkhorshid, E.; Schulten, K. *Phys. Rev. Lett.* **2004**, *93*, 224501.
- (51) Hancock, N. T.; Phillip, W. A.; Elimelech, M.; Cath, T. Y. *Environ. Sci. Technol.* **2011**, *45*, 10642–10651.